The (*p, T*) Thermodynamic Behavior of *n*-Alkanoic Acids Adsorbed on Silicate Glass: Characterization of the Phase Transitions

Léon Ter Minassian* and Siro Toscani

Laboratoire de Chimie Physique et de Chimie Minérale, Faculté des Sciences Pharmaceutiques et Biologiques, Université René Descartes-Paris V, 4 Avenue de l'Observatoire, 75270 Paris Cedex 06

Received: June 29, 1999; In Final Form: September 29, 1999

A new phenomenon has been unexpectedly discovered in studying transitions between crystal phases A, B, and C of *n*-alkanoic acids mixed with ordinary glass powder. Post-melting and pre-freezing events have been observed on scanning temperature at atmospheric pressure by means of a DSC calorimeter and on scanning pressure isothermally using a piezothermal apparatus. These phenomena have been interpreted as the melting and freezing of an assembly of Langmuir−Blodgett-like films of alkanoic acids adsorbed on the glass surface. Freezings and meltings could be observed at temperatures 10 to 15 °C higher than the conventional melting point or at pressures as much as 500 bar lower than the expected melting pressures. Optical microscopy allowed the phenomenon to be observed. The glass mixtures with lignoceric acid were thoroughly investigated at two different mass fractions. At atmospheric pressure, independent of the acid content, deposition of acid on the glass surface was achieved only at the end of a slow process of adsorption requiring repeated melting and freezing cycles. In the case of a mixture containing a poor quantity of acid, the adsorption process could be controlled by the gradual diminution and disappearance of the melting and freezing peaks of the bulk acid. On the contrary, the adsorption was completed from the first rise of pressure in the case of the piezothermal scans. In addition, both scan types showed the occurrence of new transitions after the completion of surface melting. They have been attributed to the transformation of the surface crystal into liquid-crystal-like structures onto the glass surface. In piezothermal scans, the pressure range within which transitions occurred became wider with increasing temperature.

1. Introduction

The solid crystalline structures and the phase transitions of alkanoic acids have been thoroughly studied. Early studies dealing with even carbon number alkanoic acids recognized the existence of three crystal phases (A, B, and C) prepared by crystallizations from melts in contact with solid surfaces.[1] Later on, the preparation of crystal phases from evaporated solutions has been preferred[2] because of its reproducibility. As a matter of fact, it is difficult to observe the crystallization of all three phases from the melt in a single temperature or pressure scanning. Tentatively, a mixture of myristic acid and ordinary glass was coarsely ground in a mortar and studied through pressure scanning. Our purpose was trying to trap embryos of A, B, and C phases in order to grow the corresponding crystals in their respective pressure−temperature stability ranges. We obtained a positive result that we tried to improve by using finely divided glass powder obtained by ball milling. Surprisingly, in the experiment thereafter named "primary experiment", a completely different phenomenon was observed: an after-melting effect occurred in the liquid phase region. The systematic study of the phenomenon revealed that this after-melting effect becomes more and more important as the number of carbon atoms of the even alkanoic acids increases from C_{18} to C_{24} . In this paper we describe the different aspects of the phenomenon in the case of lignoceric acid (C_{24}). This observed new effect turned out to be much more interesting than was the study of the transitions between the solid bulk phases, since it had never been investigated before under a thermodynamical point of view.

* Corresponding author.

2. Experimental Section

2.1. The Experimental Methods. The experimental approach was essentially calorimetric and performed with two different devices. The first one was a T. A. Instruments DSC 10 differential scanning calorimeter allowing temperature scans at ordinary pressure (1 bar). It provided significant determinations of the enthalpy changes associated with the aforementioned effects at a scan rate as low as 0.1 K/min on samples of about 10 mg. The claimed accuracy for enthalpy changes at melting is at least 5% after DSC energy calibration; for less energetic transitions such as a solid−solid transition accuracy is worse (10−15%), as expected. The second device was a homemade apparatus designed by one of us (L.T.M.) to determine the heat transfer when pressure is varied in isothermal conditions. It is an application of the piezothermal method which has been described elsewhere,[3,4,5] allowing the determination of the thermal expansivity as a function of pressure *p*. It has been widely implemented in the case of investigations on liquids and liquid mixtures, but, in the case of solids, technical difficulties concerning homogeneous transmission of pressure remained to be solved. This aspect has been achieved by reducing the dimensions of the sample so that pressure is uniformly applied throughout. The masses, *m*, of the samples were about 15 mg. The basic experimental equations are derived from a straightforward application of one of Maxwell's thermodynamic equations

$$(\partial S/\partial p)_T = -(\partial V/\partial T)_p \qquad (1)$$

where *S* and *V* are the molar entropy and the molar volume,

10.1021/jp992229a CCC: $18.00
Published on Web 12/01/1999

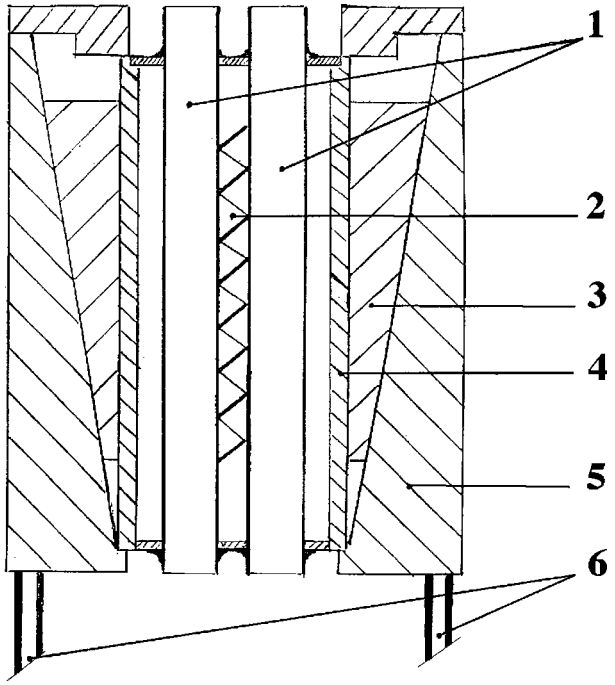

Figure 1. The piezothermal fluxmeter: (1) tubular guide, (2) set of thermocouples, (3) conical grip holder, (4) sleeve of the calorimetric cell, (5) duraluminium metallic box, (6) tubular columns.

respectively. The isothermal heat transfer δq, referred to a unit mass of sample, may be written as

$$\delta q = -T(\partial v/\partial T)_p \mathrm{d}p \tag{2}$$

where v is the specific volume. For a pressure scan, we get

$$J = -T(\partial v/\partial T)_p(\mathrm{d}p/\mathrm{d}t) \tag{3}$$

where $\delta q = J\mathrm{d}t$, where J is the heat flux relative to a unit mass of sample and $\mathrm{d}p/\mathrm{d}t$ is the rate of scan. The latter may be fixed to be equal to the constant value B. Let j be the heat flux relative to the sample mass m, the practical equation of the device may be so written as follows:

$$(\partial v/\partial T)_p = -j/(mTB) \tag{4}$$

with $j = Jm$.

N.B. The equation of Maxwell (eq 1) was originally formulated for a single phase. It has been recently shown that for a two-phase system in thermodynamic equilibrium the equation of Maxwell remains valid when V and S refer to one mole of mixture.[6]

2.2. The High-Pressure Experimental Device. The setup derived from eq 4 is designed to operate from atmospheric pressure up to 6000 bar (600 MPa) and from room temperature up to 220 °C. The heat-sensitive part is a fluxmeter (Figure 1) composed of a heavy cylindrical metallic box containing two tubular parallel guides positioned on both parts of its axis. The guides are electrically isolated and thermally connected by means of a set of thermocouples arranged in series and forming the detector element. The metallic box is positioned vertically along the axis of a heating chamber so that the sample cell could be introduced from beneath into one of the guides, whereas the other is equipped with a dummy element for thermal equilibrium. The sample cell (2.1 mm internal diameter and 8 mm height) (Figure 2a) is a heavy walled tube made of heat-treated steel and designed to be easily fitted into the fluxmeter guide.

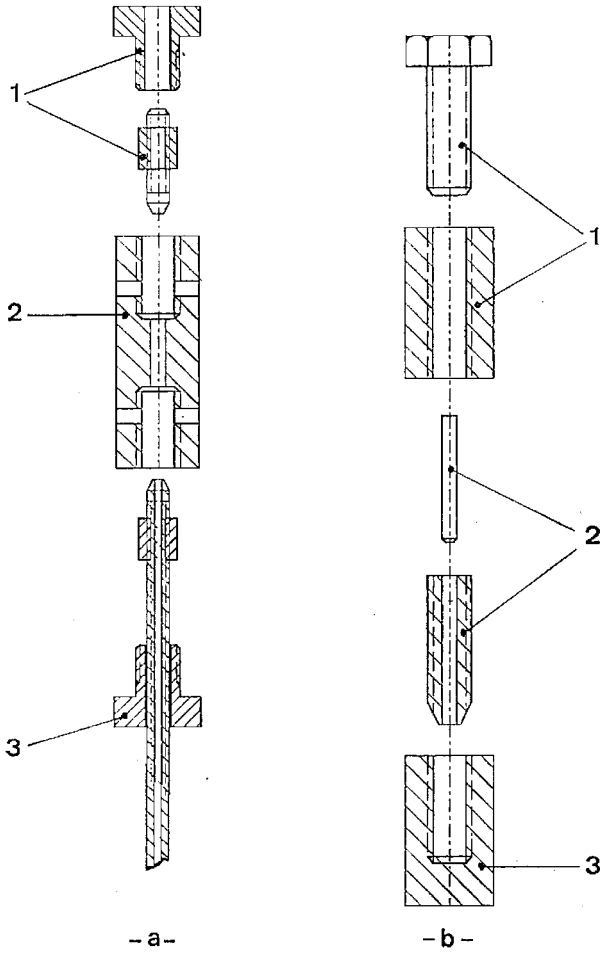

Figure 2. The sample cell and the compacting device. (a) Assembly of the cell: (1) high-pressure closure, (2) sample cell (ϕ = 11 mm, h = 30 mm), (3) high-pressure tube (ϕ_{ext} = 3.2 mm, ϕ_{in} = 1 mm). (b) The compacting device: (4) screw jack, (5) cylinder and plunger, (6) closure.

It permits the introduction of a 2 mm diameter sample. The upper side of the sample cell is equipped with a conventional closure, whereas the bottom is fitted to a high-pressure tube connected to the high-pressure equipment. The high-pressure transmitting medium is mercury and the pressure is determined through one of a set of two manometer gauges. The mechanical part of the equipment is composed of the following series of elements: a stepping motor, a gear box, a magnetic clutch, and a plunger-driven high-pressure pump. The f.e.m. of the manometer gauge and of the fluxmeter, respectively, are measured by means of a Keithley 181 nanovoltmeter, and the data were centralized into a computer which also drives the pressure regulation.

2.3. Materials. Myristic acid (purity 99.5%) was purchased from EGA-Chemie (Germany) and lignoceric acid (purity >99%) was supplied by Fluka (Germany). The ordinary glass was received from Prolabo (France) and had the following composition: SiO_2 80.8%, Na_2O 9.5%, the remaining 9.7% being constituted of a mixture of CaO and MgO.

2.4. Experimental Procedure. Coarse glass powder is prepared by crushing the glass sample with pestle and mortar; then it is ball-milled for 30 min into a fine powder. Microscopy revealed the presence of agglomerated thin flakes and BET adsorption measurement gave specific surface values varying between 200 and 400 m^2/g. The mixtures are then prepared by weighing the appropriate proportions of alkanoic acid and glass powder which are ball-milled together for 30 min. The powdered

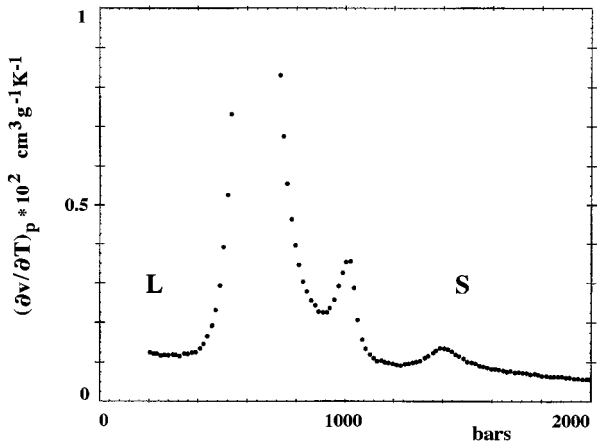

Figure 3. Piezothermal profile of the $(\delta v/\delta T)_p$ vs p scan ($T = 70.2$ °C) on decreasing pressure at a −500 bar/h rate, on a myristic acid−coarse glass powder mixture ($x = 0.641$).

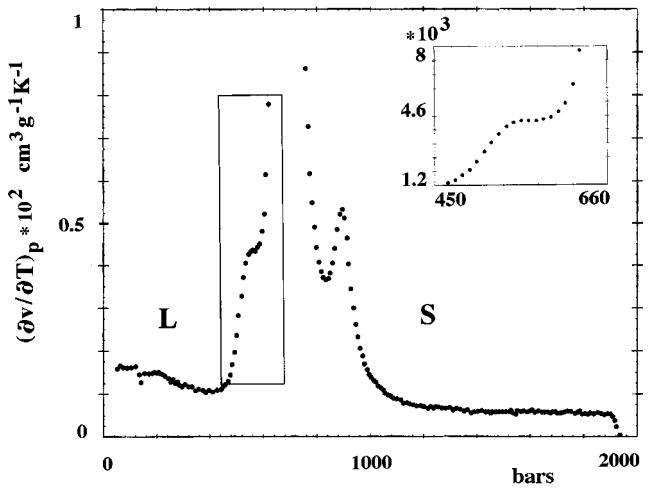

Figure 4. Piezothermal profile of the $(\delta v/\delta T)_p$ vs p scan ($T = 70.1$ °C) on decreasing pressure at a −500 bar/h rate, on a myristic acid−fine glass powder mixture ($x = 0.630$).

mixture is compacted using the device of Figure 2b. The cylinder with its plunger is then screwed onto the sample cell and the transfer is achieved by pushing the emergent part of the plunger. Weighing before and after the operation gives the mass of the transferred sample. When the transfer has been performed, the sample cell is fitted with its closure and connected to the pressure device through the high-pressure tube. An appropriate set of valves allows vacuum to be established in the system and, after a while, mercury to be admitted into the evacuated space. The highest pressure is applied and the heating chamber temperature is set according to the experimental isotherm. The measurements are performed at the constant rate of 200 or 500 bar/hour, which often leads to overnight recordings from 2000 bar to 30 bar and back to the initial high pressure.

Finally, all recordings of $(\partial v/\partial T)_p$ as a function of p are fitted by the rational interpolation method known as multipoint Padé approximate. For this purpose we use an algorithm developed by Werner[7] which determines the analytical expression of the experimental function. The latter is a rational fraction which can be deconvoluted into a sum of terms as explained in the appendix. In the case of a diagram with interweaving peaks, the procedure allows to determine the contribution of each to the overall effect.

The accuracy on entropy change is claimed to be 1%; however, uncertainty is somewhat increased in the cases when application of the deconvolution method is key, as in the treatment of overlapping peaks; it is thought to increase also with diminishing peak intensity (up to 20%).

3. Results

3.1. Primary Experiment: Myristic Acid (C_{14}). This experiment was performed in order to check the efficiency of glass powder in triggering the solid-phase transformations of myristic acid. By decreasing pressure the mixture prepared with coarse grain powder is seen (Figure 3) to induce transitions which may be identified according to the expected sequence from phase A to liquid, i.e.: A→ B→ C→ liquid. Performing the same experiment with fine powder led to the unexpected finding drawn on Figure 4. By decreasing pressure, a solid−solid transition occurred before the main melting peak followed by a well-defined kink extending in the liquid region. The experiment is reproducible and is at the origin of the present work. The post-melting phenomenon is enhanced when the chain length is increased, so that among the even carbon numbered alkanoic acids we could study, we focused on the case of lignoceric acid. In what follows, we present our observations resulting from temperature and pressure scans performed with the bulk and with two different acid−glass powder mixtures at the weight concentrations of acid of $x = 0.634$ and $x = 0.358$.

3.2. Bulk Lignoceric Acid (C_{24}). At atmospheric pressure, the melting temperature of pure lignoceric acid is $T_f = 82$ °C. The variation of melting pressure p with temperature T is given by the following equation: $(\partial p/\partial T)_{fus} = 39.0$ bar/K. Temperature scan at atmospheric pressure and isothermal pressure scans allowed to determine the melting entropies at 82 °C, 95 °C, and 110 °C, respectively. The corresponding values are 248.7, 252.7, and 248.6 J/K/mol. Thus, by application of the Clapeyron equation, the melting volumes turn out to be 63.5, 64.5, and 63.4 cm^3/mol. As expected, they remain rather constant with varying pressure and temperature on the melting line.

3.3. Acid−Glass Powder Mixture ($x = 0.634$). In the case of temperature scans, reproducible results are obtained after performing melting and freezing cycles. The temperature and pressure scans recorded on Figures 5a and 6a, respectively, show a well-defined peak before the occurrence of the freezing peak when, starting from the liquid state, the freezing temperature is approached by decreasing temperature and the freezing pressure is approached by isothermally increasing pressure. The inverse process of melting by increasing temperatures or decreasing pressures is shown in Figures 5b and 6b, respectively, and is followed by an extended post-melting effect. The likeness between melting (Figures 5b and 6b) and freezing (Figures 5a and 6a) curves, respectively, is quite remarkable. Furthermore, it may be noticed that melting and freezing occur at the same temperature, in the case of a temperature scan, and at the same pressure, in the case of pressure scan, as in the case of the bulk acid experiments.

3.4. Acid−Glass Powder Mixture ($x = 0.358$). The preceding mixture was found to contain a large excess of free acid which could have partially screened the effects implying the glass surface. In the case of a lower acid content in the mixture, we shall present separately the results obtained by means of the DSC technique and of the piezothermal one.

3.4.a Results from the Temperature Scan. Systematic heating and cooling cycles were performed at the low scan rates (0.5 K/min for the first three cycles and 0.1 K/min for the following ones). This procedure showed decreasing areas of the normal melting and freezing peaks together with the growth of post-melting and pre-freezing events, suggesting slow desorption and

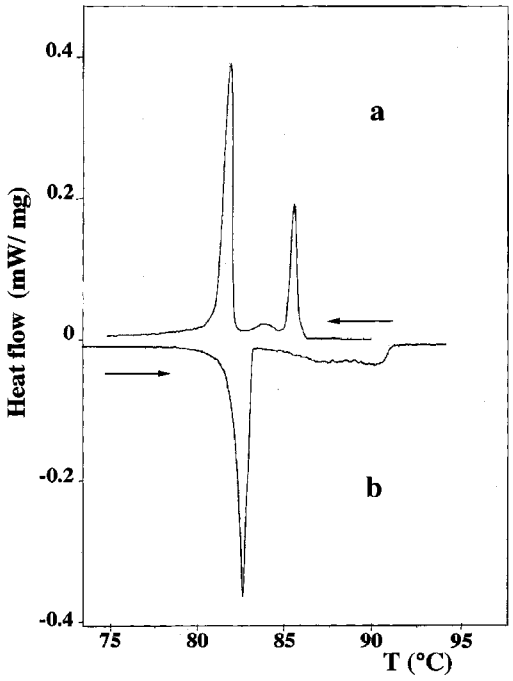

Figure 5. DSC profile of the (mW/mg) vs T scans ($p = 1$ bar), at a 0.1 K/min rate on a lignoceric acid−fine glass powder mixture ($x = 0.634$): (a) on decreasing temperature; (b) on increasing temperature.

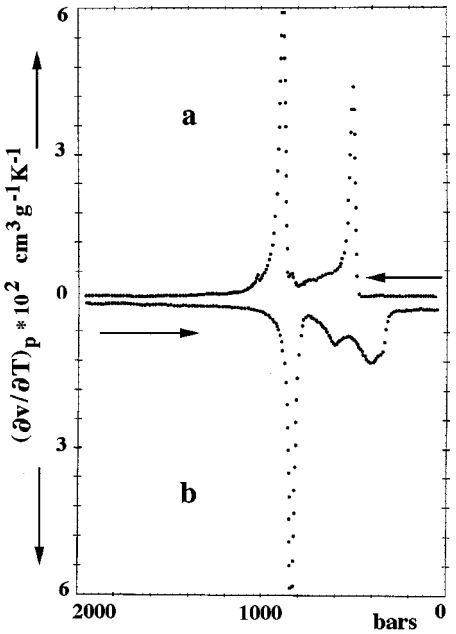

Figure 6. Piezothermal profile of the $(\delta v/\delta T)_p$ vs p scans ($T = 95$ °C) at a 200 bar/h rate on a lignoceric acid−fine glass powder mixture ($x = 0.634$): (a) on increasing pressure; (b) on decreasing pressure.

readsorption processes from and over the glass surface, respectively. These phenomena were enhanced during the first four cycles, probably because of the continuous migration of the acid molecules from the bulk liquid phase toward the adsorption sites. Starting from the fifth cycle, further cycling showed no significant further changes to what concerned temperature and enthalpy of transitions. The diagram in Figure 7a, exhibits a DSC scan performed by decreasing temperatures from 107 °C during the third cycle. Three peaks at 94.3 °C, 90.6 °C, and 87.3 °C may be observed, which precede the peak (much smaller than in Figure 5a) of the partial normal crystallization of the bulk acid (onset at 78.2 °C). The magnitude of this last one referring to the mass of acid is $\Delta H = -8.8$ kJ/mol, while the

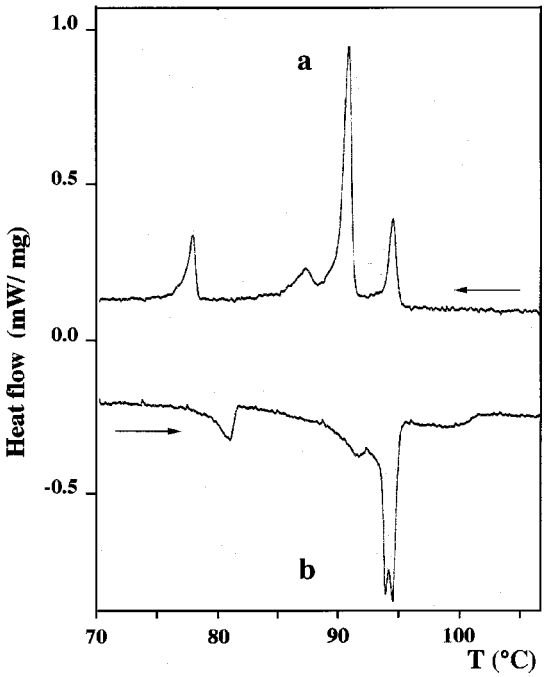

Figure 7. DSC profile of the (mW/mg) vs T scans ($p = 1$ bar) of the third heating−cooling cycle at a 0.5 K/min scan rate on a lignoceric acid−fine glass powder mixture ($x = 0.358$): (a) on decreasing temperature; (b) on increasing temperature.

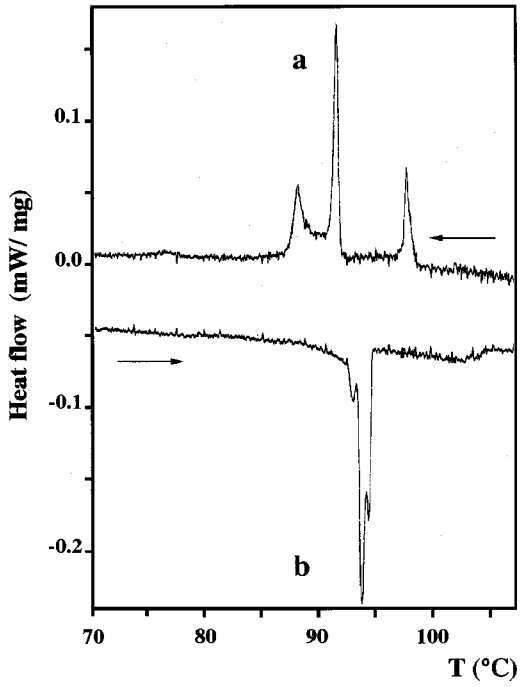

Figure 8. DSC profiles of the (mW/mg) vs T scans ($p = 1$ bar) of the fifth heating cooling cycle at a 0.1 K/min scan rate on a lignoceric acid−fine glass powder mixture ($x = 0.358$): (a) on decreasing temperature; (b) on increasing temperature.

overall enthalpic effect is of $\Delta H = -77.3$ kJ/mol, the absolute value of which is not far from 88.3 kJ/mol found for the melting of the pure acid. The diagram in Figure 7b shows the scan by increasing temperature during the same cycle. The peak of the conventional melting point of the bulk liquid is observed at 79.0 °C with an enthalpy increment of $\Delta H = 8.1$ kJ/mol, followed by a series of endothermal peaks: a small peak whose maximum is at 91.6 °C, a double peak with maxima at 93.9 °C and 94.5°C, and a very sluggish event ranging from 95.4 °C up to 101 °C.

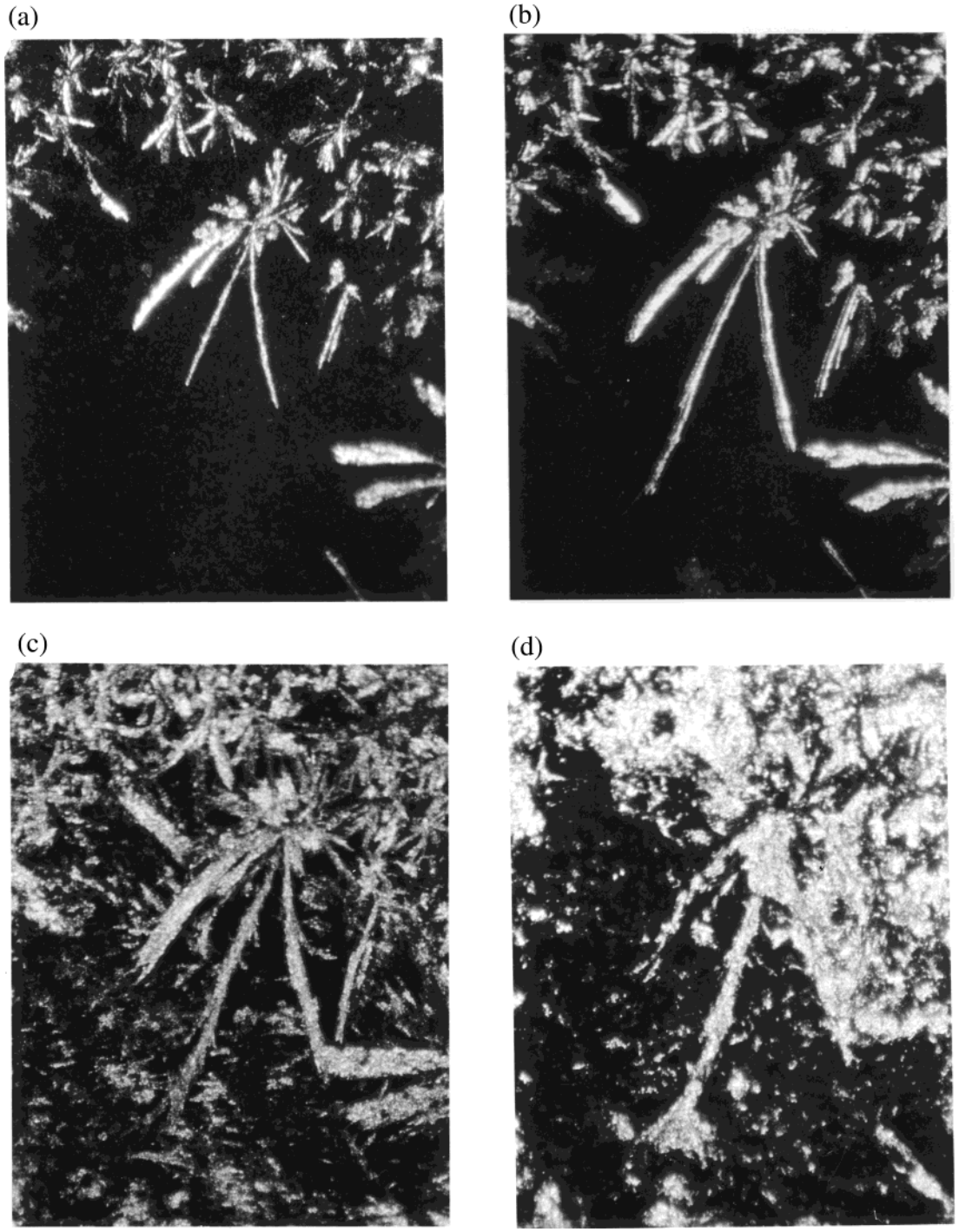

Figure 9. Microscopic observations under polarized light ($G \times 70$) of a lignoceric acid−fine glass powder mixture ($x = 0.358$): (a) cooled to 95 °C, nucleation of an adsorbed liquid crystal λ phase; (b) after stabilization at 95 °C, growth of the λ phase; (c) after further cooling to 92 °C, surface crystallization of an adsorbed solid σ phase; (d) kept at room temperature after cooling, a loss of crystallinity can be noticed.

At this stage, it is useful to compare these results with those obtained during the fifth cycle (Figure 8a). On cooling, the first peak occurs at 97.5 °C, the more exothermal peak at 91.4 °C, which is partially merged with another exothermal one at 88.0 °C, whereas the expected peak of the normal crystallization has rather disappeared. By increasing temperatures (Figure 8b), the conventional melting peak is apparently absent, whereas a triple peak is observed between 92 °C and 95 °C whose maxima are 92.8, 93.6, and 94.3, respectively. The sluggish endothermal effect is observed between 94.7 and 104°C: its associated enthalpy ($\Delta H = 17.9$ kJ/mol) is near to the absolute value of that ($\Delta H = -18.7$ kJ/mol) of the peak at 97.6 °C preceding the main exothermal peak at 91.4 °C on the cooling trace. This last peak is attributed to the beginning of the surface crystallization in agreement with microscopic observations dealt with in section 3.4.c. The triple peak on the heating trace exhibits an enthalpy value ($\Delta H = 56.2$ kJ/mol) very near to the absolute value of the sum of the two crystallization peaks (ΔH=-55.0 kJ/mol); so, it was attributed to the converse melting phenomena, which are presumably preceded by a solid−solid transition between two adsorbed phases, as the small peak at 92.8 °C seems to indicate.

3.4.b Results from Pressure Scans. We shall focus our comments on decreasing pressures scans, since by increasing

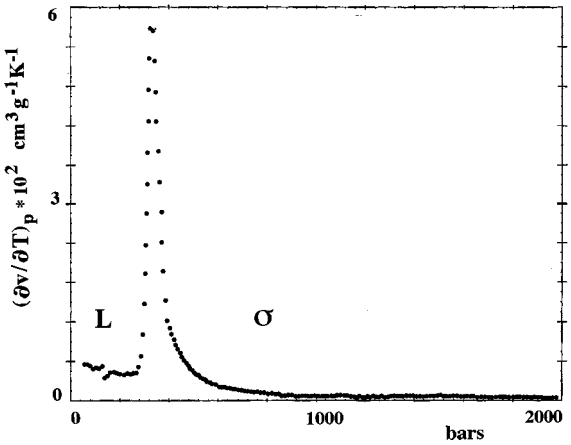

Figure 10. Piezothermal profile of the $(\delta v/\delta T)_p$ vs p scan ($T = 105.1$ °C), on decreasing pressure at a −200 bar/h rate, on a lignoceric acid−fine glass powder mixture ($x = 0.358$).

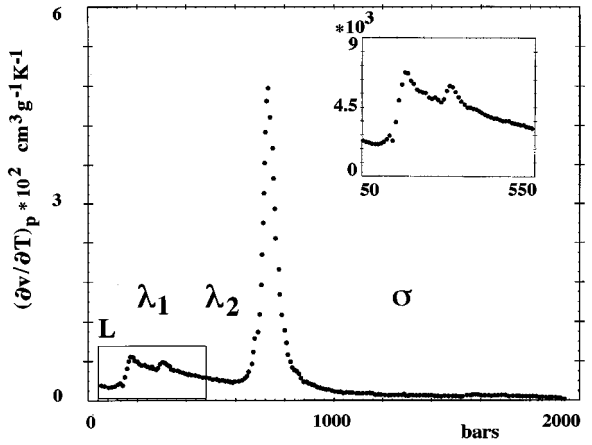

Figure 11. Piezothermal profile of the $(\delta v/\delta T)_p$ vs p scan ($T = 115.1$ °C) on decreasing pressure at a −200 bar/h rate on a lignoceric acid−fine glass powder mixture ($x = 0.358$).

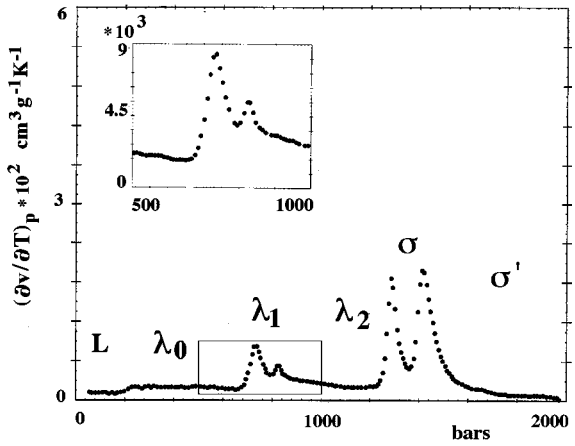

Figure 12. Piezothermal profile of the $(\delta v/\delta T)_p$ vs p scan ($T = 129.8$ °C) on decreasing pressure at a −200 bar/h rate on a lignoceric acid−fine glass powder mixture ($x = 0.358$).

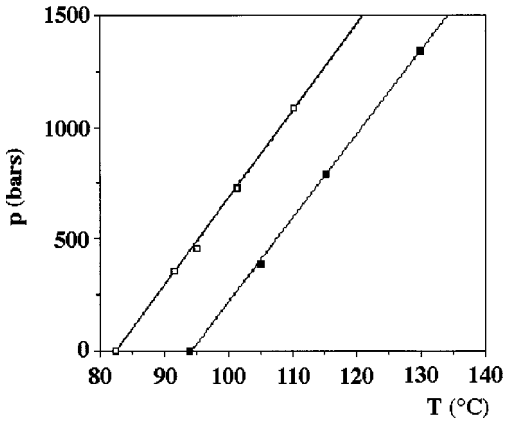

Figure 13. The melting pressures (□) of the solid bulk phase of the lignoceric acid and the melting pressures (■) of an adsorbed solid phase σ interpolated as function of temperature.

pressures the phenomenon is nucleation dependent and disconnected regions of the intergranular space may crystallize at different pressures, giving rise to unreliable results.

A piezothermal scan is performed at the temperature of 105.1 °C. By decreasing pressures, a unique peak is observed (Figure 10) at 392 bar instead of the 850 bar as could be expected for the pure acid melting. So, this peak was attributed to the occurrence of a surface melting of an adsorbed solid phase. The concerned phases were labeled L and σ, respectively, where L indicates the bulk liquid and σ the surface crystalline phase. For comparison, the experiment performed at the same temperature on the $x = 0.634$ mixture exhibits an after-melting peak at the same pressure. However, its aspect is different and reveals the occurrence of a complex mechanism.

At 115.1 °C, the surface-melting peak (Figure 11) is recorded at 788 bar (instead of 1250 bar for the normal melting point) and is followed by a sluggish heat effect (near 350 bar) corresponding to a transformation between two phases that we will call λ_1 and λ_2. Finally, near 170 bar, phase λ_1 transforms into a state which is probably the bulk liquid phase L.

At a still higher temperature, 129.8 °C, the transition of the surface solid state to phase λ_2 occurs through two well-defined peaks with onsets lying at 1515 and 1345 bar, respectively (Figure 12). Although the overall intensity of the above two peaks is smaller than that of the peak at 788 bar in Figure 11, it seems that they correspond to the splitting of the latter one as a consequence of the appearance of a second adsorbed solid phase σ'. The peak at 1515 bar could be ascribed to a $\sigma' \rightarrow \sigma$ transition, the representative point of the peak at 1345 bar being situated on the interpolated (p, T) straight line of the σ melting (Figure 13). According to a second hypothesis, the former should instead be due to the melting of the σ' phase. In this eventuality, at 129.8 °C, the adsorbed solid state of lignoceric acid could be made of a mixture of σ and σ' phases which melt independently one from another to give the same liquid phase λ_2. This interpretation may be supported if one admits the presence of noncorrelated confined regions in which each phase can be trapped. If this is the case, the adsorbed phases σ and σ' would be neither in contact nor, a fortiori, in equilibrium, one with respect to the other. Our DSC scans recorded at increasing temperature provide an interesting information since the third cycle (Figure 7a) indicates the occurrence of three peaks at 91.6 °C, 93.9 °C, and 94.5 °C. The last two peaks can be attributed to the melting of two different phases σ and σ', while the other peak may be assigned to the transformation into one of them of a third phase σ''. Repeated cycles cancel this "anomaly" since one of the phases is necessarily the metastable relative to the other and would gradually transform into the thermodynamically stable phase, as was observed by us after that sample was kept several weeks at room temperature before being reheated.

It is also shown in Figure 12 that, on further decreasing pressure, the $\lambda_2 \rightarrow \lambda_1$ transition occurred at about 840 bar, exhibiting a small peak which merged with a better marked one detected at a slightly lower pressure (around 760 bar). This last

TABLE 1: Transition Entropies in $\Delta S/R$ Units, Calculated from Piezothermal Scans on an Acid−Glass Powder Mixture ($x = 0.354$) at Three Different Temperatures

	105.1 °C		115.1 °C		129.8 °C	
transitions	p (bar)	$\Delta S/R$	p (bar)	$\Delta S/R$	p (bar)	$\Delta S/R$
$\sigma' \rightarrow \lambda_2$					1515	6.7
$\sigma \rightarrow \lambda_2$	392	18.6	788	15.3	1345	5.6
$\lambda_2 \rightarrow \lambda_1$			307	0.5	871	0.2
$\lambda_1 \rightarrow \lambda_0$					792	1.9
$\lambda_0 \rightarrow$ L					234	0.6
$\lambda_1 \rightarrow$ L			178	1.9		
background		9.1		11.1		14.6
overall		27.7		28.8		29.6
overall − background		18.7		17.7		15.0

peak was attributed to a transition of λ_1 into a third λ phase we named λ_0 . Finally, the baseline displacement at around 200 bar could be reasonably ascribed to the passage to the bulk liquid phase L.

The transition entropies $\Delta S/R$, determined from the aforementioned deconvolution method, are listed in Table 1. One may observe, when temperature increases, the decrease of the entropies of the $\sigma \rightarrow \lambda_2$ transitions together with an important increase of the entropy associated with the background.

3.4.c Microscopic Observations. Observation through polarized light when cooling the liquid phase at a −0.2 K/min scan rate brings additional information on the pre-freezing phenomenon which occurs at atmospheric pressure. Keeping in mind the melting point of the pure acid (82 °C), Figure 9a shows the appearance of structures at a temperature as high as 95.7 °C. The growth of the structure could be stopped by a temperature increase of a few degrees (up to 97 °C) allowing time for the photographic exposure. In Figure 9b, the picture taken at the same magnification shows the growth of the structure when returning to the initial temperature and back to 97 °C. Figure 9c shows that a new structure formed at the temperature of 92 °C in the black domains of 9b, whose growth could be stopped by increasing temperature up to 93.5 °C. Figure 9d gives the general aspect of the sample at room temperature. We should note on the latter a partial loss of crystallinity, which has been confirmed by X-ray powder diffractometry, that shows the presence of amorphous domains. This series of figures has been interpreted as follows: since optically active growing domains appeared (Figure 9a) at a temperature higher than that of the surface melting, they should be acknowledged as the appearance of an adsorbed λ phase, indicating the existence of surface liquid crystals. This result fully agrees with the DSC evidence of an exothermal peak at about 97 °C preceding the peaks of surface crystallizations. Figure 9b has been accounted for as the growth of this phase over its nucleation path. Figure 9c shows the surface crystallization leading to the first solid adsorbed phase σ. No evidence of a second crystallization at 88 °C has been noticed. Finally, the partial loss of crystallinity in Figure 9d could tentatively be explained as follows: at the surface crystallization, the aliphatic chains of the acid are all perpendicularly oriented with respect to the plane of the glass sites and attached to them by the −COOH groups; at room temperature, the volume contraction brings about the entanglement of these chains one over the other and a consequent increase of disorder, although they remain attached to the sites. By newly heating to melting temperature, the ordered arrangement of the chains is restored. This argument is accounted for by the experimental results: when samples, after a thermal cycle between 70 °C and 100 °C and after cooling and storage at room temperature, are reheated, they exhibit surface melting as when they are recurrently heated during a DSC cycle. On heating, no recrystallization is recorded between room temperature and 70 °C.

4. Discussion

4.1. An Analytical Survey of the Transformations. Temperature and pressure scans are similar for the sample with $x = 0.634$ acid concentration. Minor differences appear between temperature and pressure scans on the second sample ($x = 0.358$) since the resolution of the piezothermal technique is better than that of DSC and may overcome some blurring of the transitions due to inhomogeneities in the samples. We will consider mainly melting experiments for reasons of measurement reproducibility.

It seemed reasonable to introduce, together with the common liquid L, one or more phases λ consisting of liquid lignoceric acid involved in the interaction with the glass surface. We named the solid phase at the highest pressures σ, except in the case of the pressure scan at 129.8 °C (Figure 11), where another phase, σ' has been observed.

At atmospheric pressure, it can be considered that the deposition of lignoceric acid on the glass surface is a slow process of adsorption: the procedure requires repeated melting and freezing cycles during which the advancement of adsorption can be experimentally controlled via the vanishing of the melting peak of the bulk acid. On the contrary, in isothermal conditions under pressure, the adsorption seems immediate as no melting of the bulk acid is observed from the first pressure scan. This aspect does not change the fact that *in fine* analogous structures seem to form.

The plot of $\sigma \rightarrow \lambda_2$ transition pressures as a function of temperature can be interpolated with a straight line (Figure 13). Its extrapolation to $p = 1$ bar defines a point at 94.4 °C which is close to the corresponding one determined by DSC at atmospheric pressure (94.0 °C). The slope of the melting line is found to be $(\partial p/\partial T)_{fus} = 37.8$ bar/K. This supports the hypothesis according to which the $\sigma \rightarrow \lambda_2$ transitions correspond to a melting process. In this case, it should be necessary to reconcile the fact that the pressure scan at the lowest temperature (105.1 °C) involves a $\sigma \rightarrow \lambda_2$ melting entropy (18.6 e.u.) much greater than the sum (12.3 e.u.) of the two melting entropies determined at the highest temperature (129.8 °C) for the $\sigma \rightarrow \lambda_2$ and $\sigma' \rightarrow \lambda_2$ transitions. In fact, at 129.8 °C, the double mechanism of melting $(\sigma + \sigma') \rightarrow \lambda_2$ leads to the λ_2 phase, whereas the transformations $\sigma \rightarrow \lambda_2 \rightarrow$ L merge together at lower temperature, as seen for the 105.1 °C isotherm. This would confer some sort of priority to melting and would explain why the melting pressures as a function of temperature lay on a straight line which is the true coexistence line of the $\sigma \rightarrow \lambda_2$ transition. Since we deal with a true coexistence line and the general aspect of the transformation is that of a single peak, we may apply the Clapeyron equation and calculate the related volume variation. Since the entropic background occurs in the narrow range of pressure occupied by the main peak, the entropies of each are added in order to get the overall effect. With $\Delta S/R = 27.7$ e.u. (see Table 1), we have $\Delta V(\sigma \rightarrow L) = 60.9$ cm^3/mol, which is close to that calculated for the melting of the bulk acid ($\Delta V(S \rightarrow L) = 63.4$ cm^3/mol).

The occurrence of two phases, of which one is metastable, might explain the double melting peak observed in most of the DSC scans on the $x = 0.358$ mixture and in the decreasing pressure scan at the highest temperature (Figure 12). In this last case, their contribution to the overall entropy of melting is rather equal and cannot be attributed to any phase transformation. In fact, we would deal with two coexisting phases, and each one exhibits its own melting at a given pressure.

If one admits the melting entropy increment of the metastable σ' phase to be nine-tenths of that of the stable phase σ (as usually observed in DSC studies on substances exhibiting polymorphism), it is easy to estimate the mass fraction x_σ of the latter in the solid mixture from the $\Delta S/R$ values of Table 1. The calculated mass fraction is $x_\sigma = 0.4$ and consequently, the melting entropy increment for the sole σ phase would be

$$\Delta S/R\ (\sigma \rightarrow \lambda_2) = 12 \text{ e.u.}$$

Taking into account of the slope of the coexistence line, the volume variation at the $\sigma \rightarrow \lambda_2$ transition may be estimated to be

$$\Delta V(\sigma \rightarrow \lambda_2) = 26.4 \text{ cm}^3/\text{mol}$$

Thus, considering that $\Delta V(\sigma \rightarrow \text{L})$ similar to $\Delta V(S \rightarrow \text{L})$ should remain almost constant along the surface melting line, one may use the value computed for the 105.1 °C isotherm to calculate by difference the volume increment accompanying the sluggish transformation of phase λ_2 to give an ordinary wetting liquid L. Its value turns out to be 35 cm^3/mol. This finding may reflect the gain of additional degrees of freedom of the acid molecules associated with this transformation.

4.2. On the Nature of the Acid-on-Glass Deposited Surface. The disappearance of the melting and crystallization peaks involving the bulk phases of the acid at 82 °C, when its mass fraction is reduced from $x = 0.634$ to $x = 0.358$, shows that a limit exists in the coverage of the glass surface. In fact, assuming the glass surface to be equal to about 300 m^2/g and taking for an aliphatic chain a nominal area of 20 Å^2, a rough estimation based on the mixture compositions shows that the ratio of the surface area of the acid to that of the powdered glass is 1.88 for the mixture with the higher acid concentration and 0.60 for the other one. Hence, this shows that for the $x = 0.358$ mixture the critical quantity necessary for the saturation of the adsorption sites on the glass surface was still not attained. Conversely, in the case of the $x = 0.634$ mixture, an excess of acid molecules remained in the bulk phases.

The glass sites must involve the presence of the metallic ions Na^+, Ca^{2+}, and Mg^{2+}, since DSC experiments performed on a lignoceric acid−glassy quartz mixture with a mass fraction x of the acid equal to 0.358 gave neither post-melting nor prefreezing effects. Approaching the fundamental question of the interaction of the fatty acid with the surface (i.e., with the metallic ions), we should discard any irreversible reaction leading to the formation of salts in the bulk phase. It is known that sodium, calcium, or magnesium salts of long-chain fatty acids either melt at temperatures at least 100 °C higher than those of the related acids or chemically decompose before or during melting. In the first occurrence, fusion of the lignocerates would have been observed by us at temperatures (at least 200 °C) much higher than those we measured for the surface melting; in the second case, independent of the melting temperature, thermal cycles performed on these salts would have given irreversible events, different from those described here. We should rather consider weak interactions with energies of an order of magnitude of a hydrogen bond sticking the acid carboxylic group onto a site occupied by a metallic ion. This would confer an orientational order, announcing the growth of a monolayer of parallel molecules more or less perpendicular to the glass surface.

On the other hand, alkanoic acids may organize into different phases σ, as has been shown in the case of Langmuir−Blodgett films of arachidates on silicon[8]. The occurrences of vertical chains "bonded to the surface with only one oxygen atom", or of tilted chains "perfectly chelated with both oxygen on the surface" have been described. In fact, one may imagine "tilting transitions" on the surface, as has been suggested.[9] Owing to the lamellar structure of the bulk crystals of the A, B, and C main phases, one may think of the possibility of finding similar structures on the surface.

Recently, a melting transition of a Langmuir−Blodgett film of cadmium arachidate on mica or on thermally oxidized silicon substrates[10] has been discovered. The authors observed, by atomic force microscopy as a function of temperature, changes in molecular arrangements similar to the changes we observed by optical microscopy in the same temperature range. By experiments on increasing temperature, they pointed out the existence of a 2D smectic phase followed by a hexatic phase. In fact, a great variety of situations may occur on an interface. For example, no less than five different phases have been identified by X-ray technique in the case of behenic acid (C_{22}) monolayers at the air/water interface.[11]

Unlike conventional Langmuir−Blodgett films, which are thermodynamically closed and which concentrations are predefined constants, the system we deal with is a thermodynamically open system where an adsorbed phase is in equilibrium with the bulk and the surface concentration is solely determined by the (p, T) variables. Nevertheless, since crystallization and melting of lignoceric acid occurred at a temperature higher than that of the bulk phase (for melting, 94 °C instead of 82 °C at ordinary pressure), we concluded that we had obtained a Langmuir−Blodgett-like layer exhibiting the same melting and transformation properties as those described in ref 10.

Two and possibly three transitions were observed by us in the after-melting region λ occurring over the high entropy background. Phase identification would be outside the scope of this paper. However, the possible existence of liquid crystals in the λ domain would bring a suitable interpretation of our observations, since the entropies of transition between λ phases are found to be of a correct order of magnitude (Table 1).

5. Conclusion

The thermodynamic results presented in this paper are compatible with the idea that acid molecules in glass powder mixtures behave as an assembly of Langmuir−Blodgett-like films. Closely related to these films, the determination brings a new insight on the limits of stability of surface crystals. However, the process of surface melting and the ensuing formation of the λ adsorbed liquid phases are not yet quite clear since it mixes the formation and transition of surface liquid crystal phases together with liquid desorption. A comprehensive study should be achieved which would integrate the molecular interactions with the surface. Moreover, adsorption and desorption in relation to wetting aspects should also be considered in further theoretical and experimental investigations.

Acknowledgment. We thank Prof. René Ceolin (Laboratoire de Chimie Physique et de Chimie Minérale, Faculté de Pharmacie, Université de Paris V) for having supported this work and for helpful discussions and Prof. Gérard Boureau (Laboratoire de Chimie Physique, Université de Paris VI) for his suggestions and encouragement. Dr. Henri Szwarc (Laboratoire de Chimie Physique des Matériaux Amorphes, Université de Paris XI − Orsay) revised the manuscript, and we are also indebted to him for his appropriate remarks. The authors are also grateful to M. F. Gardette for her daily efficient help, and,

also, they are indebted to P. and B. Barberi (Societé SCERES − Orsay) for their gift of a specially designed calorimetric cell.

Appendix

The method of fitting high-pressure data points with a rational function has been published previously by one of us.[5] A complementary method is presented here, allowing the deconvolution of intricate independent contributions into a unique sum of terms.

Let $G(x)$ be the experimental curve of a recording with one or more maxima. A set of j points is selected arbitrarily along the curve. Let their coordinates be $(h_1, x_1)...(h_j, x_j)$. The number and position of the selected points will depend on the type of representation one has to deal with. If the representation is a rational fraction of a polynomial of degree k at the numerator and a polynomial of degree m at the denominator, k/m, then the number of points should be $j = k + m + 1$.

The mathematics for the deconvolution will pass through the following steps:

(1) The algorithm of Werner. By this algorithm, a sensible selection of points determines a continuous and derivable function $f(x)$, such that $f(x_1) = h_1$, $f(x_2) = h_2$,...,$f(x_j) = h_j$. It is a rational function which may be written as follows:

$$f(x) = \frac{a_0 + a_1x + ... + a_kx^k}{b_0 + b_1x + ... + b_mx^m} \equiv \frac{N(x)}{D(x)} \qquad \text{(A1)}$$

(2) For $k \geq m$, polynomial division brings eq A1 into the following form:

$$f(x) = q(x) + \frac{R(x)}{D(x)} \qquad \text{(A2)}$$

where $q(x)$ and $R(x)$ are polynomials of the $(k - m + 1)$th and $(m - 1)$th order, respectively.

(3) All coefficients of $f(x)$ are real, and the roots of polynomial $D(x)$ are real or complex conjugates. Determining the roots allows to write $f(x)$ as follows:

$$\frac{R(x)}{D(x)} = \frac{R(x)}{(c_0 + c_1x + c_2x^2)(d_0 + d_1x + d_2x^2)(e_0 + e_1x)...} \qquad \text{(A3)}$$

(4) The deconvolution is over when the coefficients (C_0, C_1), (D_0, D_1), E_0,... are determined in the following sum of terms:

$$\frac{R(x)}{D(x)} = \frac{C_0 + C_1x}{c_0 + c_1x + c_2x^2} + \frac{D_0 + D_1x}{d_0 + d_1 + d_2x^2} + \frac{E_0}{e_0 + e_1x} \qquad \text{(A4)}$$

This is always possible by cross multiplication of the members of eq A4 and by the identification of the coefficients of the same power of x.

(5) Let $\psi_1(x)$, $\psi_2(x)$, ..., ψ_i, ..., $\psi_n(x)$ be the terms of the sum in eq A4. They are known functions of x and may be drawn in the morphogram as independent contributions to the expansivity coefficient α. Each term would contribute to the variation of entropy by the integrated quantity $\Delta\Sigma_i$ which is determined algebraically. It is often necessary to assemble two of the functions ψ_i into a single function, $\psi_{i+j} = \psi_i(x) + \psi_j(x)$, to reproduce the shape of a transition. The contribution to entropy of such a transition would therefore be written as $\Delta\Sigma_{i+j} = \Delta\Sigma_i + \Delta\Sigma_j$.

(6) The results given in Table 1 are computed from the following number (j) of points selected all over the increasing pressure range of the diagrams: (a) 105.1 °C, $j = 8$, $k/m = 3/4$; (b) 115.1 °C, $j = 16$, $k/m = 7/8$; (c) 129.8 °C, $j = 24$, $k/m = 11/12$.

References and Notes

(1) Thibaud, J. F. *Dupré La Tour. C. R.* **1930**, *190*, 68.
(2) Nissim, G.; Kiyotaka, S. *Crystallisation and Polymorphism of Fats and Fatty Acids.* Surfactants Science series. Vol. 31. Marcel Dekker Inc.: New York and Basel, 1988.
(3) Petit, J. C.; Ter Minassian, L. *J. Chem. Thermodyn.* **1974**, *6*, 1139.
(4) Ter Minassian, L.; Pruzan, P. *J. Chem. Thermodyn.* **1977**, *9*, 375.
(5) Alba, C.; Ter Minassian, L.; Denis, A.; Soulard, A. *J. Chem. Phys.* **1985**, *82*, 384.
(6) Tomaszkiewicz, I.; Ter Minassian, L. *J. Phys. Chem.* **1988**, *92*, 6824.
(7) Werner, H. *Lectures Notes Math.* **1979**, *76*, 257.
(8) Stöhr, J. *Nexafs Spectroscopy*; Springer-Verlag: Berlin, Heildelberg, New York, 1992.
(9) Peterson, I. R.; Brzezinski, V.; Kenn, R. M.; Steitz, R. *Langmuir* **1992**, *8*, 2995.
(10) Sikes, H. D.; Schwartz, D. K. *Science* **1997**, *278*, 1607.
(11) Kenn, R. M.; Böhm, C.; Bibo, A. M.; Peterson, I. R.; Möhwald, H.; Als-Nielsen, J.; Kjaer, K. *J. Phys. Chem.* **1991**, *95*, 2092.